THE JOURNAL OF PHYSICAL CHEMISTRY Letters

Letter

pubs.acs.org/JPCL

Effect of Carrier Thermalization Dynamics on Light Emission and Amplification in Organometal Halide Perovskites

Kai Chen,[#] Alex J. Barker,[#] Francis L. C. Morgan, Jonathan E. Halpert,* and Justin M. Hodgkiss*

The MacDiarmid Institute for Advanced Materials and Nanotechnology and School of Chemical and Physical Sciences, Victoria University of Wellington, P.O. Box 600, Wellington 6140, New Zealand

Supporting Information

ABSTRACT: The remarkable rise of organometal halide perovskites as solar photovoltaic materials has been followed by promising developments in light-emitting devices, including lasers. Here we present unique insights into the processes leading to photon emission in these materials. We employ ultrafast broadband photoluminescence (PL) and transient absorption spectroscopies to directly link density dependent ultrafast charge dynamics to PL. We find that exceptionally strong PL at the band edge is preceded by thermalization of free charge carriers. Short-lived PL above the band gap is clear evidence of nonexcitonic emission from hot carriers, and ultrafast PL depolarization confirms that uncorrelated charge pairs are precursors to photon emission. Carrier thermalization has a profound effect on amplified stimulated emission at high fluence; the delayed onset of optical gain we resolve within the first 10 ps and the unusual oscillatory behavior are both consequences of the kinetic interplay between carrier thermalization and optical gain.

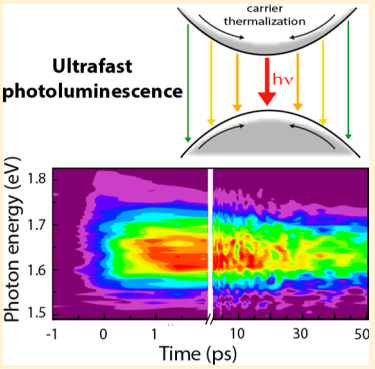

Organometal halide perovskites of the form $CH_3NH_3PbX_3$ (X = I, I/Cl, Br, Br/Cl) have rapidly emerged as one of the most promising new optoelectronic materials due to a unique combination of optical and electronic properties.[1−4] This family of materials was first investigated in the 1990s for light-emitting devices (LEDs)[5] and has recently returned to prominence as the active layer in solar photovoltaic (PV) cells,[6−9] with efficiencies rapidly climbing to ∼20%.[10] Recent reports of low-threshold amplified stimulated emission[11] (ASE) and lasing[12] and of perovskite-LEDs[13] have highlighted the additional opportunities for high-performance optical devices using the same $CH_3NH_3PbI_{3-x}Cl_x$ material. The unique combination of efficient PV and light-emission properties marks a new paradigm for optoelectronic materials and points to novel excited-state behavior.

Optical spectroscopy has already delivered several important insights into the photophysics of these materials. Low exciton binding energies[14−16] and high dielectric constants[17,18] promote photogeneration of free charge carriers[19] that obey band-filling behavior[20] and diffuse over long distances.[21,22] Charge recombination is predominantly bimolecular[12,20] and results in efficient, homogeneously broadened photon emission,[23] which exhibits femtosecond spectral relaxation[24] as well as optical gain under high fluence.[11,12] Nevertheless, details of the processes leading to photon emission remain unclear. Open questions include how the onset of PL and ASE are affected by charge formation, charge density, and dynamic band-filling behavior, and whether excitons play a role. Here we use ultrafast broadband PL spectroscopy complemented by transient absorption (TA) to explore the link between charge dynamics and the emergence of PL and ASE. By resolving the density-dependent dynamics of charges (via TA) and emissive species (via PL), these methods allow us to identify features associated with rapid charge dissociation, hot carrier emission, and thermalization, followed by intrinsically strong PL near the band edge. Furthermore, in the ASE regime, we observe that the delayed onset of gain within the first 10 ps is limited by carrier thermalization to the band edge, a kinetic interplay that also results in unusual oscillatory behavior.

We fabricated samples of $CH_3NH_3PbI_{3-x}Cl_x$ grown on a mesoporous scaffold of ∼50 nm Al_2O_3 nanoparticles using previously reported solution-processing methods,[7] as detailed in the Supporting Information. We begin by exploring the sensitivity of broadband TA dynamics to excitation fluence on early (femtosecond to nanosecond) time scales using the instrument previously described[25] (further details provided in the Supporting Information). The series of TA spectra in Figure 1a reveal three distinct spectral features: (i) a short-lived sharp absorption feature just below the edge of the linear absorption spectrum at 1.6 eV, (ii) a positive ground-state bleach (GSB) feature peaked around the band edge, and (iii) a broad feature with negative $\Delta T/T$ at photon energies > 1.75 eV. As described later, the dynamics of these spectral features are explained by rapid charge formation and thermalization. These TA measurements lead to new insights when correlated with our PL measurements of the same samples.

The shape and position of the negative feature at 1.6 eV is consistent with electroabsorption (EA) from the electric field of correlated (geminate) photogenerated charge pairs.[12] The EA decays on a ∼600 fs time scale over a wide range of excitation

Received: December 1, 2014
Accepted: December 16, 2014
Published: December 16, 2014

DOI: 10.1021/jz502528c
J. Phys. Chem. Lett. 2015, 6, 153−158

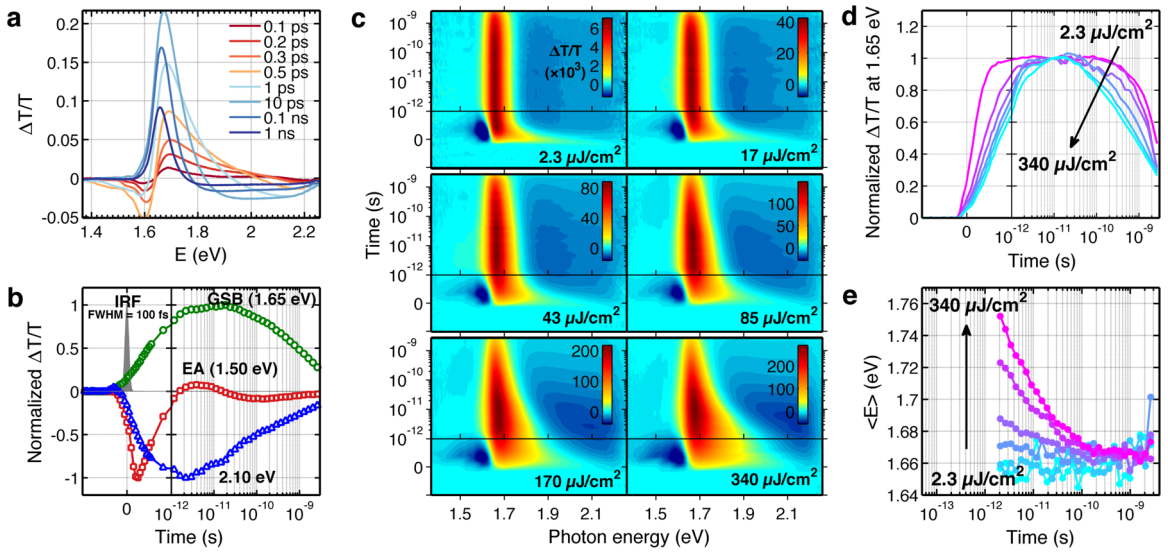

Figure 1. (a) Series of TA spectra at various times following 400 nm (3.1 eV) excitation at high fluence (170 μJ/cm^2). (b) Kinetics at various wavelengths for the same data as in part a, along with the instrument response function (IRF). (c) Broadband TA surfaces for a range of fluences of 400 nm (3.1 eV) excitation. Fluence dependence of (d) GSB dynamics probed at 1.65 eV and (e) GSB expectation energy dynamics.

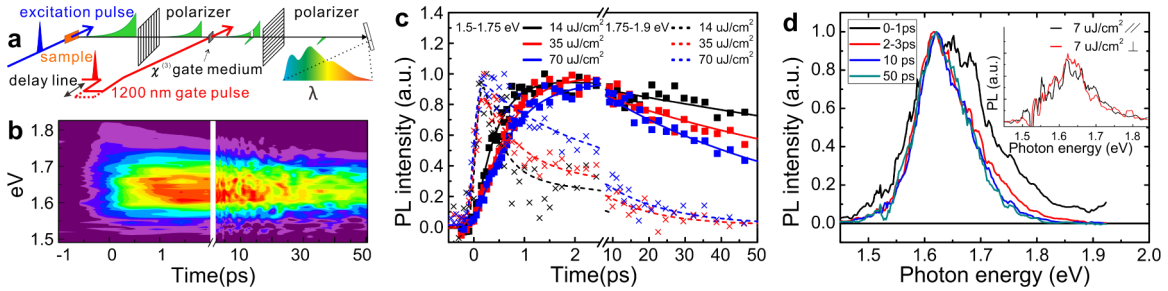

Figure 2. (a) Operation of optical Kerr gate ultrafast broadband PL shutter. (b) Ultrafast PL spectral dynamics after 600 nm (2.07 eV) excitation (70 μJ/cm^2). (c) Normalized PL kinetics for various spectral windows as a function of excitation fluence. (d) Normalized PL spectra at various integration times after 600 nm (2.07 eV) excitation (70 μJ/cm^2). The inset shows polarization-resolved PL spectra at 100 fs under weak 600 nm excitation (7 μJ/cm^2).

densities (Supporting Information), placing an estimate on the time scale of free charge carrier formation that broadly agrees with the transient terahertz absorption signal observed to peak at ~2 ps in $CH_3NH_3PBI_3$.[19] The decay of the broad negative $\Delta T/T$ peak at energies >1.75 eV commensurate with the GSB peak shows that it is associated with free charges; however, its early time appearance is obscured by overlapping GSB. The overlapping TA signals and possible further implications are addressed in the Supporting Information.

The GSB signal dominates the TA profile. Manser and Kamat probed intensity-dependent dynamics of the GSB peak to show that its spectral width (when the GSB is maximized around 5 ps) is well-described by the Burstein−Moss model of electronic band filling.[20] The fluence-dependent TA dynamics we measured, illustrated by the series of contour plots in Figure 1c, leads us to augment this picture with information about thermalization dynamics. While the GSB feature is peaked around the band edge, it grows at the expense of a high-energy tail that disappears at early times and is not included in the quasi-equilibrium Burstein−Moss analysis. At low fluence, the narrowing time scale (~1 ps) roughly coincides with the disappearance of EA and the appearance of the high-energy negative feature at energies above 1.75 eV. However, increasing the excitation density makes it clear that the two dynamics are not directly linked. In Figure 1c, the series of TA surfaces show that higher fluences result in substantially prolonged spectral narrowing, while EA dynamics are virtually unaffected (see the Supporting Information). We attribute the dynamic spectral narrowing to intraband carrier thermalization, which has greater amplitude at increasing carrier density.

Figure 1d shows the growth of the relaxed carrier population as a function of fluence via the GSB peak. At the highest fluence measured (340 μJ/cm^2), it takes >6 ps for the GSB feature to reach its maximum intensity via the relaxation of hot carriers, identified at earlier times by their high-energy GSB tail. Figure 1d also shows the subsequent density-dependent bimolecular recombination, which can occur before spectral relaxation is complete at high fluence. This can be seen by comparing the GSB decay kinetics in Figure 1d with the dynamics of spectral narrowing quantified by the GSB expectation energy in Figure 1e. Spectral narrowing has a characteristic time scale of $t_{1/2} \approx$ 10 ps. This can be regarded as the approximate thermalization time scale, noting that the plot begins from 2 ps, which is when the spectral width can be quantified after the disappearance of EA. The complementary ultrafast PL measurements described later support this interpretation, which has significant implications for the onset of optical gain. Similar density-dependent behavior is observed with 600 nm (2.07 eV) excitation over the same probe energy and time scales (see Supporting Information), noting that our probe range did not

DOI: 10.1021/jz502528c
J. Phys. Chem. Lett. 2015, 6, 153−158

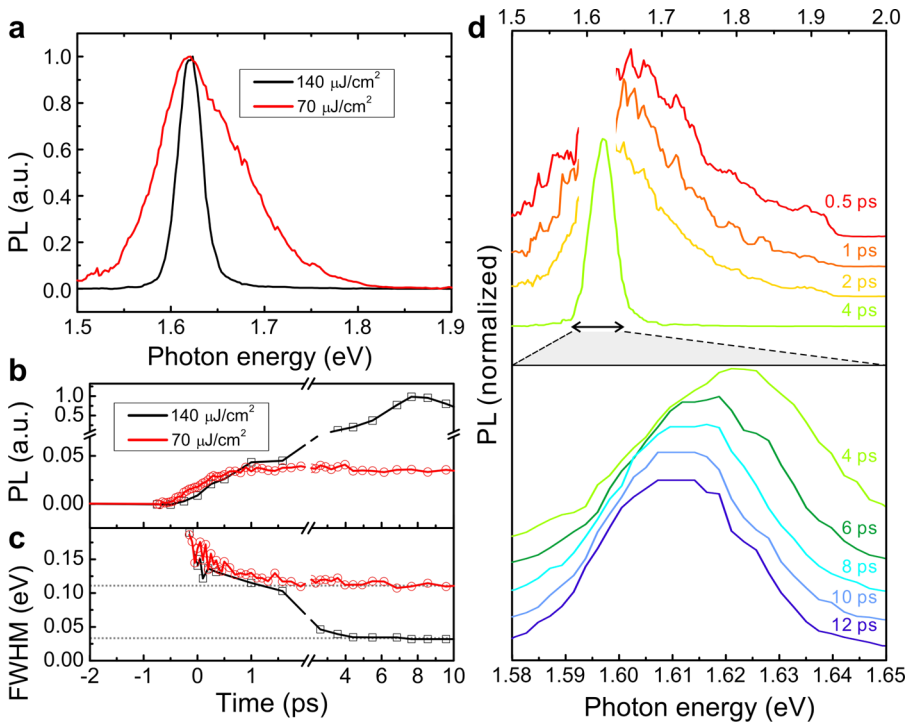

Figure 3. Ultrafast PL dynamics of $CH_3NH_3PbI_{(3-x)}Cl_x$ above the ASE threshold. (a) Normalized steady-state PL spectra at excitation fluences below and above the ASE threshold. (b) Time resolution of the ASE onset via PL dynamics integrated over 1.45 to 1.85 eV measured at excitation fluences below and above the ASE threshold. Note the compressed PL intensity scale in the ASE regime. (c) Spectral width (fwhm) dynamics for the same data sets as in part (b). (d) Time-resolved spectral dynamics tracking the onset of ASE following 600 nm (2.07 eV) excitation (140 μJ/cm^2).

extend to the higher energy GSB feature used to identify hot hole dynamics.[21]

The organometal halide perovskites are noted for their high PL quantum efficiencies, which is rare for such high-performing PV materials. These properties have led to organometal halide perovskite-based optical gain devices[11,12] and allow us to use ultrafast broadband PL spectroscopy to directly resolve the formation of emissive states and how they are affected by carrier density and thermalization dynamics. To make these measurements, we use a gated ultrafast broadband PL spectra using the optical Kerr gate technique[26] depicted in Figure 2a and further described in the Supporting Information. In brief, an optical shutter constructed from two orthogonal linear polarizers is opened when an ultrafast gate pulse transiently induces birefringence in an intervening $\chi^{(3)}$ medium. The method benefits from broadband phase-matching, making it ideal for resolving ultrafast spectral dynamics. The kilohertz rep-rate system also has sufficient pulse energy to access density-dependent effects, including ASE.

Figure 2b shows how the PL surface for the $CH_3NH_3PbI_{(3-x)}Cl_x$ sample evolves within the first 50 ps of excitation. Dynamic spectral relaxation is evident from the PL surface and the corresponding kinetics and spectra shown in Figure 2c,d, respectively, consistent with the low fluence narrow-band ultrafast PL measurements of Hsu et al.[24] High-energy PL is resolved above the band gap, which has an instrument-limited onset and subpicosecond decay at low excitation fluence (Figure 2c). PL derived from recombination of nonthermalized carriers is also evident from the subpicosecond high-energy spectral edge in Figure 2d. This effect becomes more pronounced at higher excitation fluence (see Supporting Information) as a larger proportion of charges spend several picoseconds in higher energy states. In contrast, the main PL peak at 1.63 eV exhibits delayed growth within the first 1 ps and minimal decay by 50 ps. The wavelength-dependent PL dynamics are strongly correlated with the GSB dynamics for the TA measurements previously described. This correlation persists for density-dependent measurements. Analogous to the fluence-dependent GSB dynamics above, Figure 2c shows that increased fluence results in delayed decay of the high energy PL edge and delayed rise of PL at the relaxed band edge as a result of prolonged thermalization at high excitation density. Figure 2c also shows the expected acceleration of subsequent PL decay via bimolecular recombination at high fluence.

We confirm that PL is preceded by recombination of uncorrelated charge carriers rather than geminate charge pairs by resolving the absence of ultrafast polarization anisotropy. The inset of Figure 2d reveals that the rising intensity of PL at 100 fs is equivalent for PL that is polarized parallel with and perpendicular to the excitation pulse throughout the spectrum. Thus, photogenerated charge pairs lose memory of the excitation dipole on an ultrafast time scale. In the other case, higher PL intensity in the parallel detection channel would have pointed to radiative recombination of correlated charge pairs or primary excitons that were initially polarized until diffusion occurred. We verified that this observation is not explained by PL scattering in the mesostructured sample via the neglible depolarization observed for transmission of a sub-bandgap laser beam. The correlation between fluence-dependent ultrafast TA and PL dynamics, along with ultrafast depolarization, leads us to conclude that both display the effects of thermalizing charge carriers rather than exciton relaxation dynamics invoked by Hsu et al.[24]

Because free-carrier thermalization dynamics extend beyond 10 ps (Figures 1 and 2), many charges recombine from a

DOI: 10.1021/jz502528c
J. Phys. Chem. Lett. 2015, 6, 153−158

nonthermalized state at high excitation density. This kinetic bottleneck led us to explore the implications for the onset of ASE, where these effects must be balanced at even higher fluences. In the time-integrated PL spectra in Figure 3a, we observe the substantial spectral narrowing that is the signature of ASE at high fluence.[11,12] The ASE threshold here exceeds 70 μJ/cm^2, higher than the 10 μJ/cm^2 reported by Xing et al.,[11] possibly due to a higher defect density in our air-processed mesostructured sample. The spectral position of the ASE peak confirms that carriers must thermally relax to the band edge to contribute to a population inversion. This implies that there is a higher intrinsic radiative rate at the band edge, which is further supported by the ASE dynamics discussed later.

Figure 3b,c shows the time dependence of the peak PL intensity and the fwhm when pumping above and below the ASE threshold. The two data sets are broadly similar within the first 2 ps; the rise of PL intensity at the main peak is linked to the time scale of spectral narrowing to the homogeneously broadened peak width, and both processes take slightly longer to complete at higher fluence. The onset of ASE is clearly identified by the divergence of the high- and low fluence data sets beyond 2 ps; above the ASE threshold, the peak intensity begins a second phase of growth and narrows to less than half of the thermalized fwhm found below the ASE threshold. The fact that both processes take ~8 ps to reach their limiting values is also reflected in the slight dynamic red shift observed for the ASE peak (Figure 3d). The delayed buildup of ASE is a consequence of delayed carrier thermalization to the band edge at high density, leading to ASE buildup on a similar time scale to the thermalization resolved via high fluence TA spectroscopy in Figure 1.

Figure 4 shows that we observe even slower ASE build-up times at higher fluence. Interestingly, we also see a secondary

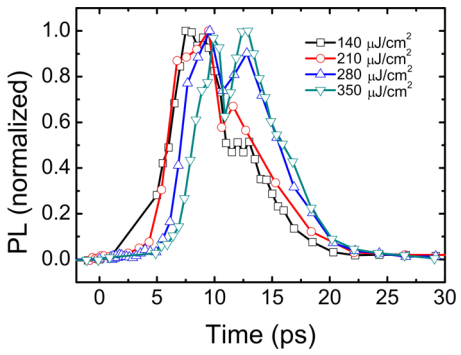

Figure 4. Temporal profiles of ASE growth and decay at various excitation fluences via the intensity integrated across 1.5 to 1.75 eV.

ASE peak emerging after the initial intensity drops. This temporal profile is repeatable and suggests that the population inversion that is rapidly depleted through ASE can be eventually regenerated with the energetic relaxation of additional hot carriers that were too high in energy to contribute to the first ASE peak. The secondary peak has greater relative amplitude at high fluence (where a larger population of hot carriers is stored above the band-edge beyond the first ASE event). A shoulder around 17 ps points to the possibility of a third ASE phase after the secondary population inversion is depleted and recovered via further carrier thermalization. This novel oscillatory behavior is a direct consequence of the kinetic interplay between thermalization-limited population inversion and rapid depletion in the ASE regime. Trapping processes may also play a role. However, trapping does not appear to be the primary reason for delayed onset of ASE. In that case, traps would be saturated to bring about ASE more quickly at high fluence, contrary to our observation. A remaining challenge is to quantify radiative and nonradiative decay rates to augment these observations with a predictive quantitative model.

The ultrafast measurements above highlight the dominant role of free charge carrier dynamics, even for PL, where photon emission is preceded by thermalization and recombination of uncorrelated charge pairs. However, it is worth considering the role of excitonic states. The absorption spectra of organometal halide perovskites feature a sharp excitonic transition just below the band edge, resulting in a higher absorption cross-section than direct interband absorption would produce, considering the lower density of states near the band edge at $k = 0$.[14] The present work adds to the unambiguous evidence that weakly bound excitonic states are rapidly dissociated to produce free carriers at room temperature.[3,14−16]

Our observation of early time PL above the band gap suggests that radiative recombination can proceed without mediation from lower energy excitonic states. However, we also found that ASE occurs only after thermalization to the band edge, despite the presence of a relatively long-lived population inversion of hot carriers at high fluence. This observation suggests that the gain coefficient, which is related to the intrinsic radiative rate, is higher at the band edge where ASE is observed. We also found that absolute time-resolved PL amplitudes exceed those measured under the same conditions for molecular excitonic systems such as conjugated polymers and oligomers.[26,27] Bound excitonic states feature high radiative recombination rates via their strong electron−hole overlap. However, as Koch et al. describe,[28,29] radiative recombination of free carriers in direct gap semiconductors can display strong optical resonances nearly identical to excitons when considering many body interactions. Indeed, their nonexcitonic theory predicts picosecond time scale PL narrowing in quantum wells[29] that is qualitatively comparable to the experimental observations we present here. Ambiguity over the role of excitons in mediating the PL in organometal halide perovskites might be resolved in the future by using terahertz absorption spectroscopy to identify resonant transitions to higher exciton levels[28] and also quantifying energy-dependent radiative rate constants for PL.

It is worth noting that the thermalization-limited delayed onset of ASE is not likely to affect the prospects of electrically pumped lasers using these materials. Carrier thermalization dynamics proceed immediately after injection from the electrodes, leaving the thermalized electron and hole populations to interact in the centrally located active layer of the device. Nevertheless, the characteristics of organometal-halide-perovskite-based LEDs[13] show that achieving sufficient densities of confined electrons and holes at the band edge remains a formidable impediment to the realization of electrically pumped organometal halide perovskite lasers.

Finally, the carrier thermalization dynamics also have important implications for solar PV applications. If an appropriate device architecture could be found to harvest hot carriers on picosecond time scales, the open-circuit voltage of the cell could be substantially increased. Although there are significant engineering challenges to hot carrier harvesting, this would have the potential to greatly improve the power

DOI: 10.1021/jz502528c
J. Phys. Chem. Lett. 2015, 6, 153−158

conversion efficiency, possibly breaking the Shockley−Queisser limit for a single junction cell.

In summary, we find that TA spectral dynamics of $CH_3NH_3PbI_{3-x}Cl_x$ are described by rapid formation of free charge carriers followed by thermalization to the band edge over ∼10 ps. Fluence-dependent PL spectral dynamics, including the observation of above gap PL at early times and high fluence, mirror the thermalization effects resolved via TA. Together with the observation of ultrafast PL depolarization, this behavior confirms that free charge carriers precede the formation of emissive states. Finally, we have shown that carrier thermalization has a profound effect on ASE; the delayed buildup of a population inversion at the band edge and the observed oscillatory behavior are both consequences of the kinetic interplay between carrier thermalization and optical gain. Ultimately, the understanding and implications of carrier thermalization dynamics presented here will enable the development of more effective optical gain and charge-harvesting schemes using these and similar organometal halide perovskite materials.

■ ASSOCIATED CONTENT

Supporting Information

Detailed sample preparation procedures, spectroscopic methods, linear absorption spectrum, further ultrafast transient absorption spectroscopy and analysis (intensity dependence of electroabsorption signal dynamics, non-normalized GSB rise at the band edge, TA spectroscopy with 600 nm excitation, separation of GSB contribution to TA spectra, analysis of apparent dynamic increase in GSB cross-section), and excitation fluence dependence of ultrafast PL spectra. This material is available free of charge via the Internet at http://pubs.acs.org.

■ AUTHOR INFORMATION

Corresponding Authors

*E-mail: Jonathan.Halpert@vuw.ac.nz.
*E-mail: Justin.Hodgkiss@vuw.ac.nz.

Author Contributions

#A.J.B. and K.C. contributed equally.

Notes

The authors declare no competing financial interest.

■ ACKNOWLEDGMENTS

J.M.H. acknowledges support from a Rutherford Discovery Fellowship and the Marsden Fund. We gratefully acknowledge Richard Friend and Michael Price for valuable discussions.

■ ABBREVIATIONS

ASE, amplified stimulated emission; EA, electroabsorption; fwhm, full width at half-maximum; GSB, ground-state bleach; IRF, instrument response function; LED, light-emitting diode; PL, photoluminescence; PV, photovoltaic; TA, transient absorption

■ REFERENCES

(1) Grätzel, M. The light and shade of perovskite solar cells. *Nat. Mater.* **2014**, *13*, 838−842.
(2) Green, M. A.; Ho-Baillie, A.; Snaith, H. J. The emergence of perovskite solar cells. *Nat. Photonics* **2014**, *8*, 506−514.
(3) Sum, T. C.; Mathews, N. Advancements in Perovskite Solar Cells: Photophysics behind the Photovoltaics. *Energy Environ. Sci.* **2014**, *7*, 2518−2534.
(4) Hodes, G.; Cahen, D. Photovoltaics: Perovskite cells roll forward. *Nat. Photonics* **2014**, *8*, 87−88.
(5) Mitzi, D. B. Synthesis, Structure, and Properties of Organic-Inorganic Perovskites and Related Materials. *Prog. Inorg. Chem.* **2007**, *48*, 1−121.
(6) Kojima, A.; Teshima, K.; Shirai, Y.; Miyasaka, T. Organometal Halide Perovskites as Visible-Light Sensitizers for Photovoltaic Cells. *J. Am. Chem. Soc.* **2009**, *131*, 6050−6051.
(7) Lee, M. M.; Teuscher, J.; Miyasaka, T.; Murakami, T. N.; Snaith, H. J. Efficient Hybrid Solar Cells Based on Meso-Superstructured Organometal Halide Perovskites. *Science* **2012**, *338*, 643−647.
(8) Kim, H.-S.; Lee, C.-R.; Im, J.-H.; Lee, K.-B.; Moehl, T.; Marchioro, A.; Moon, S.-J.; Humphry-Baker, R.; Yum, J.-H.; Moser, J. E.; et al. Lead Iodide Perovskite Sensitized All-Solid-State Submicron Thin Film Mesoscopic Solar Cell with Efficiency Exceeding 9%. *Sci. Rep.* **2012**, *2*, 1−7.
(9) Liu, M.; Johnston, M. B.; Snaith, H. J. Efficient Planar Heterojunction Perovskite Solar Cells by Vapour Deposition. *Nature* **2013**, *501*, 395−398.
(10) Zhou, H.; Chen, Q.; Li, G.; Luo, S.; Song, T.-B.; Duan, H.-S.; Hong, Z.; You, J.; Liu, Y.; Yang, Y. Interface Engineering of Highly Efficient Perovskite Solar Cells. *Science* **2014**, *345*, 542−546.
(11) Xing, G.; Mathews, N.; Lim, S. S.; Yantara, N.; Liu, X.; Sabba, D.; Grätzel, M.; Mhaisalkar, S.; Sum, T. C. Low-Temperature Solution-Processed Wavelength-Tunable Perovskites for Lasing. *Nat. Mater.* **2014**, *13*, 476−480.
(12) Deschler, F.; Price, M.; Pathak, S.; Klintberg, L. E.; Jarausch, D.-D.; Higler, R.; Hüttner, S.; Leijtens, T.; Stranks, S. D.; Snaith, H. J.; et al. High Photoluminescence Efficiency and Optically Pumped Lasing in Solution-Processed Mixed Halide Perovskite Semiconductors. *J. Phys. Chem. Lett.* **2014**, *5*, 1421−1426.
(13) Tan, Z.-K.; Moghaddam, R. S.; Lai, M. L.; Docampo, P.; Higler, R.; Deschler, F.; Price, M.; Sadhanala, A.; Pazos, L. M.; Credgington, D.; et al. Bright Light-Emitting Diodes Based on Organometal Halide Perovskite. *Nat. Nanotechnol.* **2014**, *9*, 687−692.
(14) D'Innocenzo, V.; Grancini, G.; Alcocer, M. J.; Kandada, A. R.; Stranks, S. D.; Lee, M. M.; Lanzani, G.; Snaith, H. J.; Petrozza, A. Excitons versus Free Charges in Organo-Lead Tri-Halide Perovskites. *Nat. Commun.* **2014**, *5*, 3586.
(15) Edri, E.; Kirmayer, S.; Mukhopadhyay, S.; Gartsman, K.; Hodes, G.; Cahen, D. Elucidating the Charge Carrier Separation and Working Mechanism of $CH_3NH_3PbI_{(3-x)}Cl_{(x)}$ Perovskite Solar Cells. *Nat. Commun.* **2014**, *5*, 3461.
(16) Marchioro, A.; Teuscher, J.; Friedrich, D.; Kunst, M.; van de Krol, R.; Moehl, T.; Grätzel, M.; Moser, J.-E. Unravelling the Mechanism of Photoinduced Charge Transfer Processes in Lead Iodide Perovskite Solar Cells. *Nat. Photonics* **2014**, *8*, 250−255.
(17) Juarez-Perez, E. J.; Sanchez, R. S.; Badia, L.; Garcia-Belmonte, G.; Kang, Y. S.; Mora-Sero, I.; Bisquert, J. Photoinduced Giant Dielectric Constant in Lead Halide Perovskite Solar Cells. *J. Phys. Chem. Lett.* **2014**, *5*, 2390−2394.
(18) Gonzalez-Pedro, V.; Juarez-Perez, E. J.; Arsyad, W. S.; Barea, E. M.; Fabregat-Santiago, F.; Mora-Sero, I.; Bisquert, J. General Working Principles of $CH_3NH_3PbX_3$ Perovskite Solar Cells. *Nano Lett.* **2014**, *14*, 888−893.
(19) Ponseca, C. S., Jr.; Savenije, T. J.; Abdellah, M.; Zheng, K.; Yartsev, A.; Pascher, T.; Harlang, T.; Chabera, P.; Pullerits, T.; Stepanov, A.; et al. Organometal Halide Perovskite Solar Cell Materials Rationalized: Ultrafast Charge Generation, High and Microsecond-Long Balanced Mobilities, And Slow Recombination. *J. Am. Chem. Soc.* **2014**, *136*, 5189−5192.
(20) Manser, J. S.; Kamat, P. V. Band Filling with Free Charge Carriers in Organometal Halide Perovskites. *Nat. Photonics* **2014**, *8*, 737−743.
(21) Xing, G.; Mathews, N.; Sun, S.; Lim, S. S.; Lam, Y. M.; Grätzel, M.; Mhaisalkar, S.; Sum, T. C. Long-Range Balanced Electron- And

DOI: 10.1021/jz502528c
J. Phys. Chem. Lett. 2015, 6, 153−158

Hole-Transport Lengths in Organic-Inorganic $CH_3NH_3PbI_3$. *Science* **2013**, *342*, 344−347.
(22) Stranks, S. D.; Eperon, G. E.; Grancini, G.; Menelaou, C.; Alcocer, M. J. P.; Leijtens, T.; Herz, L. M.; Petrozza, A.; Snaith, H. J. Electron-Hole Diffusion Lengths Exceeding 1 Micrometer in an Organometal Trihalide Perovskite Absorber. *Science* **2013**, *342*, 341−344.
(23) Wehrenfennig, C.; Liu, M.; Snaith, H. J.; Johnston, M. B.; Herz, L. M. Homogeneous Emission Line Broadening in the Organo Lead Halide Perovskite $CH_3NH_3PbI_{3-x}Cl_x$. *J. Phys. Chem. Lett.* **2014**, *5*, 1300−1306.
(24) Hsu, H.-Y.; Wang, C.-Y.; Fathi, A.; Shiu, J.-W.; Chung, C.-C.; Shen, P.-S.; Guo, T.-F.; Chen, P.; Lee, Y.-P.; Diau, E. W.-G. Femtosecond Excitonic Relaxation Dynamics of Perovskite on Mesoporous Films of Al_2O_3 and NiO Nanoparticles. *Angew. Chem.* **2014**, *126*, 9493−9496.
(25) Barker, A. J.; Chen, K.; Hodgkiss, J. M. Distance Distributions of Photogenerated Charge Pairs in Organic Photovoltaic Cells. *J. Am. Chem. Soc.* **2014**, *136*, 12018−12026.
(26) Chen, K.; Barker, A. J.; Reish, M. E.; Gordon, K. C.; Hodgkiss, J. M. Broadband Ultrafast Photoluminescence Spectroscopy Resolves Charge Photogeneration via Delocalized Hot Excitons in Polymer:-Fullerene Photovoltaic Blends. *J. Am. Chem. Soc.* **2013**, *135*, 18502−18512.
(27) Chen, K.; Gallaher, J. K.; Barker, A. J.; Hodgkiss, J. M. Transient Grating Photoluminescence Spectroscopy: An Ultrafast Method of Gating Broadband Spectra. *J. Phys. Chem. Lett.* **2014**, *5*, 1732−1737.
(28) Koch, S. W.; Kira, M.; Khitrova, G.; Gibbs, H. M. Semiconductor Excitons in New Light. *Nat. Mater.* **2006**, *5*, 523−531.
(29) Kira, M.; Jahnke, F.; Koch, S. W. Microscopic Theory of Excitonic Signatures in Semiconductor Photoluminescence. *Phys. Rev. Lett.* **1998**, *81*, 3263−66.

DOI: 10.1021/jz502528c
J. Phys. Chem. Lett. 2015, 6, 153−158